

# 1 Southward Shift of the Northern Tropical Belt from 1945 to 1980

2

3 Stefan Brönnimann<sup>1,2</sup>, Andreas M. Fischer<sup>3</sup>, Eugene Rozanov<sup>4,5</sup>, Paul Poli<sup>6</sup>, Gilbert P. Compo<sup>7,8</sup>, Prashant  
4 D. Sardeshmukh<sup>7,8</sup>

5

6 <sup>1</sup> Oeschger Centre for Climate Change Research, Univ. Bern, Switzerland

7 <sup>2</sup> Institute of Geography, Univ. Bern, Bern, Switzerland

8 <sup>3</sup> Federal Office of Meteorology and Climatology MeteoSwiss, Zurich, Switzerland

9 <sup>4</sup> Physical-Meteorological Observatory/World Radiation Center PMOD/WRC, Davos, Switzerland

10 <sup>5</sup> Institute for Atmospheric and Climate Sciences, ETH Zurich, Switzerland

11 <sup>6</sup> European Centre for Medium-Range Weather Forecasts ECMWF, Reading, UK

12 <sup>7</sup> Cooperative Institute for Research in Environmental Sciences, Univ. Colorado, Boulder, Colorado, USA

13 <sup>8</sup> Physical Sciences Division, Earth System Research Laboratory, National Oceanic and Atmospheric Administration, Boulder,  
14 Colorado, USA

15 Published in Nature Geoscience 2015

16 **Changes in the position and width of the tropical belt are societally and ecologically relevant,**  
17 **because they are associated with shifts of the subtropical dry zones. The tropical belt has widened**  
18 **since about 1980, but little is known about its earlier variability. Here we analyse historical surface**  
19 **and upper-level observations, three global reanalysis data sets, and a reconstruction of total column**  
20 **ozone, to show that the northern tropical edge retracted from 1945 to 1980, while the northern**  
21 **Hadley cell shifted southward in both summer and winter. We present chemistry-climate model**  
22 **simulations that reproduce the retraction and southward shift. We find that retraction of the**  
23 **tropical belt was largely due to cooling sea-surface temperatures north of the equator and warming**  
24 **south of the equator, most prominently over the Atlantic. Substantial hydroclimatic anomalies such**  
25 **as European droughts of the 1940s and 1950s and the Sahel drought of the 1970s were associated**  
26 **with this shift of the Hadley cell. Our results suggest that multidecadal changes in the position of**  
27 **the northern Hadley cell are an important component of climate variability.**

28 The tropical belt is the region influenced by the meridional atmospheric circulation cell known as the  
29 Hadley cell (illustrated by the zonal mean meridional mass stream function  $\psi$  in Fig. 1 for boreal winter).  
30 Its equatorward branch is marked by the Intertropical Convergence Zone (ITCZ), a region of high  
31 precipitation and associated strong ascent of moist air. It is also a zone with often calm surface winds over  
32 the oceans (equatorial calms). At its poleward branch, air masses descend and precipitation is accordingly  
33 low. The poleward edge of the tropics can be defined in zonally-averaged meteorological fields by the  
34 positions of features (Fig. 1) such as another region of relatively calm surface winds over the ocean  
35 (subtropical calms), high sea-level pressure (subtropical highs), strong descent in the free troposphere, the  
36 subtropical jet at around 200 hPa, and the “subtropical ozone front” (a steep ozone increase towards the  
37 midlatitudes that is related to the change in tropopause altitude).<sup>1-3,6</sup>

38

### 39 **Recent tropical widening, unknown past**

40 Since the edge of the tropical belt affects the position of the subtropical dry zones, decadal shifts or trends  
41 in the tropical edge determine the transition between drought and non-drought conditions and are  
42 therefore highly relevant for society. While droughts in Australia have been attributed to the current  
43 widening of the tropical belt<sup>7</sup>, the relation of past decadal hydroclimatic changes to shifts in the tropical  
44 belt has received less attention. Here we focus on hydroclimatic changes over the period 1945-1980 as  
45 depicted in precipitation trends (Fig. 2; see Fig. S1 for significance). Southern and Central Europe were  
46 affected by severe summer drought from ca. 1945 to the early 1950s, then precipitation increased. The  
47 Southern USA suffered from drought in the early 1950s while summers got wetter in the subsequent  
48 decades. Conversely, in the Sahel region pluvial conditions prevailed in the 1950s, followed by severe  
49 drought in the 1970s (a similar pattern is found in the Orinoco basin<sup>8</sup>). Previous work has linked the Sahel  
50 drying to a southward shift of the ITCZ<sup>9,10]</sup>, but changes of the northern edge of the tropical belt and their  
51 relation to hydroclimatic anomalies have not been addressed.

52 As early as 1969, the eminent climatologist Hubert H. Lamb noted (among other climatic changes) an  
53 equatorward shift of the subpolar cyclones, subtropical anticyclones, and arid zones during the 1950s and  
54 1960s based on sea-level pressure data<sup>11</sup>. In a recent paper, Allen et al.<sup>12</sup> report a contraction of the  
55 northern tropical belt from 1950 to 1979 in climate model simulations and observation-based data

56 (Version 2 of the atmospheric reanalysis 20CR<sup>[13]</sup>). However, they found that trends are weak and  
57 ambiguous, as are trends based on other reanalyses for the 1958-1979 period<sup>14</sup>. Further evidence is thus  
58 required.

59

## 60 **A multi-evidence approach**

61 Even regarding the widening of the tropical belt since 1979, magnitudes derived from reanalyses are  
62 uncertain<sup>2,3,14,15</sup> and confidence in the widening rests on the fact that it is evident in different, independent  
63 data sets and indicators (atmospheric reanalyses, outgoing long-wave radiation, total column ozone<sup>6</sup>,  
64 among others). The availability of multiple data sets has restricted most research to the post-1979 era.

65 Recently, new data sets have been produced for earlier decades that allow a more robust view of changes  
66 in the tropical belt prior to 1979. In addition to sea-level pressure (HadSLP<sup>[16]</sup>), marine surface winds  
67 (COADS, v2.5<sup>[17]</sup>), and the surface-driven 20CR reanalysis Version 2, a new version of 20CR (Version  
68 2c) and another long, surface-driven reanalysis data set, ERA-20C, have been released<sup>18</sup>. Furthermore,  
69 two reconstructions of upper-level fields based on surface and upper-air observations (here termed  
70 REC1<sup>[19]</sup> and REC2<sup>[20]</sup>) and a reconstruction of atmospheric ozone based on assimilating ground-based  
71 and satellite total column ozone observations into chemistry-climate model simulations (HISTOZ<sup>[21]</sup>) are  
72 available. In total, eight global data sets are used in our study (note that REC2 is spatially incomplete),  
73 some of which are largely or even fully independent, thus providing a more comprehensive view than one  
74 data set alone.

75 Here we use the reanalysis data sets to calculate trends in latitude-height cross-sections of the zonal mean  
76 zonal wind  $\bar{u}$  and the zonal mean meridional stream function  $\psi$  for different seasons using least-squares  
77 regression. Trends in  $\psi$  in 20CRv2c (Fig. 3) show a dipole-like structure, with an increase (decrease) on  
78 the southern (northern) side of the maximum in both seasons, more pronounced in winter. Similar results  
79 are also found for 20CRv2 and ERA20C (Fig. S2). The dipole structure implies a southward shift of the  
80 northern Hadley cell. This is illustrated by contrasting contours of  $\bar{u}$  and  $\psi$  representative for the years  
81 1945 and 1980 as obtained with the linear trend fit. The red contours (representing 1980) of  $\psi$  lie mostly  
82 equatorward of the black contours (representing 1945) by one or even several degrees latitude. For  $\bar{u}$ , a

83 similar result is found for the winter season. A dipole trend pattern appears with a strengthening to the  
84 south and a weakening to the north of the jet maximum, implying an equatorward shift. In summer the  
85 main trend is a weakening of the jet with little displacement.

86

## 87 **Southward shift in observations and model**

88 To further address latitudinal trends in atmospheric circulation features, we used the above mentioned  
89 data sets (except ICOADS winds) in the form of monthly zonal averages to calculate indices of the  
90 tropical belt width and position (Methods and Table S2). Our indices (indicated schematically in Fig 1)  
91 capture the positions of the subtropical calms over the oceans (in ERA20C, which is the only data set we  
92 use that ingests observed surface marine winds), the subtropical highs (HadSLP, all reanalyses), the  
93 strongest descent at 500 hPa (all reanalyses), the subtropical jet (maximum of  $\overline{u}$  at 200 hPa, from REC1,  
94 REC2 and all reanalyses) and of the maximum meridional gradient of total column ozone (HISTOZ and  
95 all reanalyses). Furthermore, we also analysed the positions of the Hadley cell centre (maximum of  $\psi$  in  
96 all reanalyses) and of the ITCZ (maximum ascent at 500 hPa in all reanalyses as well as equatorial calms  
97 over the ocean in ERA20C). The monthly indices were then averaged into boreal summer (April to  
98 September) and winter (October to March) seasons and series of the same index from different data sets  
99 were averaged.

100 The data sets and measures should be assessed critically. The indices stem from different data sources and  
101 measure different aspects of tropical and subtropical circulations (Fig. 1). However, most indices are  
102 significantly correlated on an interannual scale, including those of the ITCZ position and of the tropical  
103 edge position. The subtropical high index is well correlated with other edge indices only in winter, but not  
104 in summer, while the subtropical calms and total ozone indices are well correlated with other indices in  
105 summer but not in winter (Table S1). The indices also exhibit similar long-term behaviour. Their trends  
106 confirm that the ITCZ moved southward in both seasons. This is in agreement with previous studies<sup>9,10,22</sup>,  
107 which found a southward shift of the tropical rain belt and the ITCZ during the second half of the 20<sup>th</sup>  
108 century. Our study shows that this southward shift of the ITCZ coincided with a similar southward shift  
109 of the Hadley Cell centre and of the northern tropical edge that was not previously reported. This points to  
110 a picture of wider reorganisation of the Hadley circulation that links historical shifts from drought to non-

111 drought conditions in south central Europe with shifts from non-drought to drought conditions in the  
112 Sahel.

113 All 16 calculated index trends are negative. According to a binomial test (accounting for the effective  
114 degrees of freedom  $N^*$  in the series<sup>23</sup>) the p-values for all trends having the same sign is  $p = 0.0045$ .  
115 Moreover, nine trends are statistically significant on a 95% confidence level (Fig. 4). Thus, the individual  
116 metrics and the overall picture clearly support a southward shift of the tropical belt. Depending on the  
117 index series, the best estimate for the shift amounts to 0.25-1.5° latitude over the period. The results  
118 reinforce the hypotheses of Lamb<sup>11</sup> and Allen et al.<sup>12</sup>, which can now be supported by various  
119 independent data sets.

120 These results are further confirmed by historical observations of surface marine winds (Fig. S3) and  
121 corresponding ERA-20C reanalysis data, which allow tracing the northern and southern edges of the  
122 Hadley cell as regions with near zero zonal and meridional winds, respectively (Methods). Between 1945-  
123 1954 and 1971-1980 (Fig. S3) the ITCZ moved southward in both seasons and basins. The northern edge  
124 moved southward in both seasons in the Pacific, whereas observations in the Atlantic region show a  
125 southward shift only in winter.

126 In the following, the observation-based results are compared with an initial-condition ensemble of nine  
127 simulations of the 20<sup>th</sup> century with the chemistry-climate model SOCOL<sup>[24]</sup>. The interactive chemistry  
128 allows analysing the tropical edge position in total column ozone. Simulations were performed in an “all  
129 forcings” set up (termed ALL), where sea-surface temperatures (SSTs) and sea ice<sup>25</sup>, greenhouse gases,  
130 solar irradiance, stratospheric aerosols, and tropospheric trace gas emissions were prescribed in a transient  
131 manner, while tropospheric aerosols were prescribed according to a climatology<sup>26</sup>. All indices (except for  
132 the calms, as 10 m wind speeds were not available) were calculated in the same way as in observation-  
133 based data: separately for each ensemble member, and then averaged.

134 Trends in latitude-height sections in the ensemble mean of the model simulations (Fig. 3) exhibit a  
135 southward shift of the ITCZ that is similar to that in reanalyses (note, however, that both the model and  
136 reanalyses specify the evolution of SSTs). Trends near the northern edge are not or only barely significant  
137 ( $p = 0.05$ ) in the model. A dipole-like trend pattern appears for the zonal mean zonal wind in boreal

138 winter similar to all reanalyses. In boreal summer, the agreement is worse and at the same time the  
139 differences between the reanalyses are larger (Fig. S2).

140 Indices of the latitudinal position of circulation features provide a more detailed view of tropical belt  
141 shifts in the simulations. An overview of the corresponding trends in the observation-based and model-  
142 based indices is given in Fig. 5. In the model, 11 out of 12 trends are negative (6 significant at the 95%  
143 confidence level). As for the observation-based indices, the overall picture of the negative trends in  
144 several circulation features provides evidence of an equatorward shift of the northern tropics in the model.  
145 Trends for northern tropical edge indices in summer are more variable in the model than in observation-  
146 based data. Also, the trends in the positions of descent (#6) and total column ozone increase (#8) are  
147 smaller in the model. All other trend magnitudes of model and observations are within each other's 95%  
148 confidence intervals. Model and observations are thus consistent. Studies on the recent widening found  
149 that atmospheric models forced with observed SSTs better capture the observed widening trend than  
150 coupled models, though they still strongly underestimate the trend magnitude<sup>4,12</sup>.

151 An additional ensemble of three simulations was performed in which SSTs were prescribed from a  
152 climatology representative of 1900 conditions (Methods). In order to assess the effect of SSTs on the  
153 trend, we analysed the difference of the trends between the two ensembles (blue rectangles in Fig. 5). The  
154 ensemble with climatological SSTs but transient external forcings shows mostly small poleward shifts  
155 and hence the trend difference is somewhat larger than trends in ALL. This implies that, in the model, the  
156 trends found in ALL can be explained entirely by SSTs (in the real world, the latter are of course not  
157 independent of the forcings).

158

## 159 **Decadal Oceanic Variability or Aerosols?**

160 How did the SSTs change? The main feature of the trend over the 1945-1980 period is a cooling north of  
161 the equator and a warming south of the equator, particularly in the Atlantic (Fig. 2). This pattern can also  
162 be described as a negative trend in the Atlantic Multidecadal Oscillation (AMO). Strong interhemispheric  
163 gradients in temperature trends are understood to drive the latitudinal position of the ITCZ on decadal  
164 time scales<sup>22</sup>, which is consistent with our findings. Specifically, the Sahel pluvial during the 1950s and  
165 subsequent droughts have been attributed to changes in the interhemispheric temperature gradient during

166 these decades<sup>20,27,28</sup>. Moreover, it has been shown that summer temperature and precipitation over  
167 Southern Europe<sup>29</sup> and in the USA<sup>30</sup> are affected by the AMO, which reached a strongly positive phase  
168 during the late 1940s and early 1950s. Although the relation of droughts in these regions to the low-level  
169 moisture flux and the large-scale circulation is more complex than implied in Fig. 1, the associated  
170 circulation changes are part of the tropical edge shift. Changes in hydroclimate and the tropical belt  
171 position are thus consistent with specific SST trend patterns altering the atmospheric flow and  
172 precipitation patterns<sup>31</sup>.

173 Various factors have been held responsible for the change in SSTs: Internal variability of the North  
174 Atlantic Ocean<sup>32</sup> as well as forcing due to anthropogenic aerosols<sup>33,34</sup>, which was specifically addressed in  
175 the context of Sahel drying and ITCZ shifts<sup>35,36,37</sup>. The low-frequency residual of El Niño Southern  
176 Oscillation also is expected to have played a role, particularly in the Pacific and Indian Oceans<sup>38</sup>. If future  
177 studies identify natural variability as the main cause, this implies that improvements in ocean initialisation  
178 of decadal forecasts might help to better depict future changes in the tropical edge position. If aerosols are  
179 found to play the dominant role, this points to the importance of understanding future aerosol levels in  
180 projecting future changes of SSTs and the tropical belt.

181 Our results are consistent with a shift of the northern tropical belt of about 0.25° latitude per decade, i.e.,  
182 a shift of roughly 1° in latitude over the 1945 to 1980 period. Although this amounts to only around 100  
183 km, shifts were arguably much larger regionally and was highly relevant in areas of strong precipitation  
184 gradients, as evidenced in the occurrence of severe droughts. Our findings indicate that interannual-to-  
185 multidecadal changes in the tropical belt due to changes in SSTs are an important component of climate  
186 variability. A southward shift from 1945 to 1980 also has implications for interpreting the current  
187 widening of the tropical belt, which might have started from a southward shifted state.

188 Data from the tropics and southern hemisphere are still sparse, but would allow for a more complete view  
189 of changes in the Hadley circulation in this period. Current efforts<sup>39</sup> are small steps towards Lamb's grand  
190 vision: "Knowledge of the great climatic changes of the past can help in the development of long range  
191 weather forecasts. But the work of collecting, and putting into order, sufficient data on a worldwide scale  
192 is only just beginning."<sup>[11]</sup>

193

## 194 **Methods**

### 195 **Data**

196 REC1<sup>[19]</sup> is a reconstruction of monthly hemispheric (15°-90°N) upper-level geopotential height and  
197 temperature fields from historical upper-level and surface data. It is based on principal component  
198 regression using ERA-40<sup>[40]</sup> as a target and is spatially complete, but assumes stationarity of hemispheric  
199 principal component patterns. REC1 is complemented with ERA-40 after 1957. REC2<sup>[20]</sup> is also a  
200 statistical reconstruction of monthly upper-level geopotential height, wind, and temperature from  
201 historical upper-level and surface data. It also uses principal component regression and is calibrated using  
202 ERA-40. However, REC2 is a grid-column-by-grid-column reconstruction considering only predictors  
203 from a cone of influence around that grid column and requiring a minimum amount of upper-level  
204 observations. Thus, no stationarity of spatial patterns is assumed, but grid columns away from upper-air  
205 observations have no data. We only took grid cells into account that have a complete record from April  
206 1943 onward (no gap allowed). The spatial coverage is shown in Fig. S1. This reduced data set was then  
207 zonally averaged for further processing. After 1957 REC2 was extended to 1980 using the reconstruction  
208 in the calibration period<sup>20</sup>.

209 The data set HISTOZ is based on an assimilation of historical ground-based and satellite total column  
210 ozone observations into the ALL ensemble simulations with the SOCOL chemistry climate model<sup>21</sup>. After  
211 1979, HISTOZ is supplemented by the BDBP satellite based ozone data set<sup>41</sup>.

212 The spatial resolutions of the data sets differ. REC1 and REC2 have a resolution of 2.5° longitude and  
213 latitude, 20CR has a 2° resolution, HISTOZ and HadSLP are coarser, with a resolution of 5°. SOCOL has  
214 a resolution of 3.8°. In order to keep the resolutions of the data sets similar, we used ERA-20C in a 2°x2°  
215 resolution for calculating the indices. For further analyses we also used ICOADS wind data<sup>17</sup> as well as  
216 the global GPCP precipitation data<sup>42</sup>.

217 Note that HISTOZ is entirely independent of REC1, REC2, and HadSLP. HISTOZ, REC1, and REC2 are  
218 quasi-independent of the reanalyses. HISTOZ shares with the reanalyses the dependence on model  
219 boundary conditions (including SSTs), but the increments in the northern hemisphere subtropics are  
220 substantial and HISTOZ differs significantly from the background<sup>21</sup>. REC1, REC2 and the reanalyses  
221 share sea-level pressure information, but the weight of this is strongly limited in the reconstructions.



222 The marine surface winds from ICOADS<sup>[17]</sup> provide historical observational records of atmospheric  
 223 circulation covering many regions of the globe over the time period of interest (years 1945 to 1980). A  
 224 proxy for the edges of the Hadley cell is to observe where the wind changes direction, *i.e.*, where one of  
 225 its components crosses zero. Such a signal is more robust for the wind component shifting between two  
 226 strong regimes, and over oceans, as orography affects wind over land. In Fig. S3 we show near-zero  
 227 contours for average zonal and meridional wind.

228

## 229 **Indices**

230 All indices were calculated from zonal averages of monthly fields. They are defined as the interpolated  
 231 latitude  $\varphi$  of the minimum or maximum (here  $\varphi_{min}$ ) in a variable  $x$  within a given range. Definitions based  
 232 on maxima or minima are preferred over zero-crossing positions, which may be affected more strongly by  
 233 biases.

234 The interpolation (here for  $\varphi_{min}$ ) was obtained by:

$$235 \quad \varphi_{min} = \varphi_0 - \Delta\varphi \cdot \frac{x_1 - x_{-1}}{2 \cdot |x_0 - \max(x_{-1}, x_1)|}$$

236 where subscripts 0, -1, and 1 refer to the value or latitude of the minimum (or maximum)  $x$  and its  
 237 neighbours,  $\Delta\varphi$  is the resolution.

238 Several of the analysed fields exhibit double maxima or minima not only in individual months, but even  
 239 in the climatology (e.g., vertical velocity as shown in Fig. 1). Therefore, it is important to restrict the  
 240 accepted range as carefully as possible depending on the season (see Table S2, note that due to the  
 241 different resolution of SOCOL, slightly different ranges were used in that data set). If no local minimum  
 242 (maximum) was found within the range, the corresponding edge of the range was chosen. If, in rare cases,  
 243 more than one local minimum (maximum) was found, the more equatorward one (which could include a  
 244 global minimum at the equatorward edge) was chosen for indices of the tropical edge but the global  
 245 minimum was chosen for the ITCZ indices. The following indices were used (see Fig. 1):

### 246 *Intertropical Convergence Zone (ITCZ)*

- 247 1. Strongest ascent: Maximum upward vertical velocity  $\omega$  at 500 hPa in the tropics from 20CRv2,  
 248 20CRv2c, ERA-20C, and SOCOL. Restricting the accepted range reduces ambiguities.

249 2. Equatorial calms: Latitude of lowest 10 m wind speed over the oceans near the equator in  
250 ERA20C

251 *Hadley Cell Centre*

252 3. Centre of Meridional Overturning: The latitude of the maximum of  $\psi$  in the northern tropics at  
253 any level between 500 hPa and 700 hPa in 20CRv2, 20CRv2c, ERA-20C, and SOCOL.

254 Occasionally, the maximum occurs at an even lower level, but in these there was often an  
255 ambiguity, which can be avoided by restricting the lowest level to 700 hPa.

256 *Northern Tropical Edge:*

257 4. Subtropical highs: The latitude of the maximum sea-level pressure in the subtropics in HadSLP,  
258 20CRv2, 20CRv2c, ERA-20C, and SOCOL.

259 5. Subtropical calms: Latitude of lowest 10 m wind speed over the oceans in the subtropics in  
260 ERA20C.

261 6. Strongest descent: Latitude of the maximum downward vertical velocity  $\omega$  at 500 hPa in the  
262 subtropics in 20CRv2, 20CRv2c, ERA-20C and SOCOL. At that level, ambiguities can be  
263 avoided.

264 7. Subtropical jet: Latitude of the maximum of  $\bar{u}$  at 200 hPa in the subtropics in 20CRv2, 20CRv2c,  
265 ERA-20C, REC1, REC2 and SOCOL. For REC1 we used the latitudinal gradient in zonally  
266 averaged 200 hPa geopotential height. The 200 hPa level was chosen as because those instances  
267 in which the wind maximum was not at 200 hPa were rare.

268 8. Subtropical ozone front: Maximum meridional total column ozone gradient in the subtropics in  
269 HISTOZ, 20CRv2, 20CRv2c, ERA-20C, and SOCOL.

270 The monthly indices and fields were then averaged into boreal summer (April to September) and winter  
271 (October to March) seasons. Further, we averaged the series from all different data sets.

272

273 **Model**

274 The SOCOL model<sup>24</sup> and the set-up of the ALL simulations<sup>26</sup> are described in detail in the literature.  
275 Simulations with fixed SSTs were performed starting in 1901 and using a climatology derived from  
276 observed<sup>25</sup> SSTs from 1886 to 1915. SSTs for these years were averaged after excluding the volcanically  
277 perturbed years (i.e. two years after the eruption of St. Maria in Oct. 1902 and two years after Mt. Katmai  
278 eruption in June 1912). Additionally, strong ENSO events in the 30-yr period were removed before  
279 averaging according to Table 1 in Brönnimann et al.<sup>43</sup>.

280

## 281 **References**

- 282 1. Seidel, D. J., Fu, Q., Randel, W. J. & Reichler, T. J. Widening of the tropical belt in a changing climate. *Nature Geosci.* **1**, 21–  
283 24 (2008).
- 284 2. Quan, X.-W., Hoerling, M. P., Perlwitz, J., Diaz, H. F. & Xu, T. How fast are the Tropics expanding? *J. Climate* **27**, 1999–  
285 2013 (2014).
- 286 3. Davis, S. M. & Rosenlof, K. H. Multidiagnostic Intercomparison of Tropical-Width Time Series Using Reanalyses and  
287 Satellite Observations. *J. Clim.* **25**, 1061–1078 (2012).
- 288 4. Allen, R. J., Sherwood, S. C., Norris, J. R. & Zender, C. S. Recent Northern Hemisphere tropical expansion primarily driven  
289 by black carbon and tropospheric ozone *Nature* **485**, 350–355 (2012).
- 290 5. Hartmann, D. L. *et al.* Observations: Atmosphere and Surface. In: *Climate Change 2013: The Physical Science Basis.*  
291 Contribution of Working Group I to the Fifth Assessment Report of the Intergovernmental Panel on Climate Change (Eds.  
292 Stocker, T. F. *et al.*). Cambridge University Press, Cambridge, United Kingdom and New York, NY, USA.
- 293 6. Hudson, R. D. Measurements of the movement of the jet streams at mid-latitudes, in the Northern and Southern Hemispheres,  
294 1979 to 2010. *Atmos. Chem. Phys.* **12**, 7797–7808 (2012).
- 295 7. Post, D. A. *et al.* Decrease in southeastern Australian water availability linked to ongoing Hadley cell expansion, *Earth's*  
296 *Future* **2**, doi:10.1002/2013EF000194 (2014).
- 297 8. Marengo, J. Variations and change in South American streamflow. *Climatic Change* **31**, 99–117 (1995).
- 298 9. Held, I. M., Delworth, T. L., Lu, J., Findell K. L. & Knutson, T. R. Simulation of Sahel drought in the 20th and 21st centuries.  
299 *Proc. Natl. Acad. Sci. USA* **102**, 17891–17896 (2005).
- 300 10. Hwang, Y.-T., Frierson, D. M. W. & Kang, S. M. Anthropogenic sulfate aerosol and the southward shift of tropical  
301 precipitation in the late 20th century. *Geophys. Res. Lett.* **40**, 2845–2850 (2013).
- 302 11. Lamb, H. H. The New Look of Climatology. *Nature* **23**, 1209–1215 (1969).
- 303 12. Allen, R. J., Norris, J. R. & Kovilakam, M. Influence of anthropogenic aerosols and the Pacific Decadal Oscillation on  
304 tropical belt width. *Nature Geosci.* **7**, 270–274 (2014).
- 305 13. Compo, G. P. *et al.* The Twentieth Century Reanalysis Project. *Q. J. R. Meteorol. Soc.* **137**, 1–28 (2011).

- 306 14. Lu, J., Deser, C. & Reichler, T. Cause of the widening of the tropical belt since 1958. *Geophys. Res. Lett.* **36**, L03803 (2009).
- 307 15. Birner, T. Recent widening of the tropical belt from global tropopause statistics: Sensitivities. *J. Geophys. Res.*, **115**, D23109
- 308 (2012).
- 309 16. Allan, R. & Ansell, T. A New Globally Complete Monthly Historical Gridded Mean Sea Level Pressure Dataset (HadSLP2):
- 310 1850-2004. *J. Clim.* **19**, 5816-5842 (2006).
- 311 17. Woodruff, S. D. *et al.* ICOADS Release 2.5: extensions and enhancements to the surface marine meteorological archive. *Int.*
- 312 *J. Climatol.* **31**, 951-967 (2011).
- 313 18. Poli, P. *et al.* *The data assimilation system and initial performance evaluation of the ECMWF pilot reanalysis of the 20th-*
- 314 *century assimilating surface observations only (ERA-20C)*. ERA Report Series 14, ECMWF, Reading (2013).
- 315 19. Griesser, T. *et al.* Reconstruction of global monthly upper-level temperature and geopotential height fields back to 1880. *J.*
- 316 *Clim.* **23**, 5590–5609 (2010).
- 317 20. Brönnimann, S., Griesser, T. & Stickler, A. A gridded monthly upper-air data set from 1918 to 1957. *Clim. Dynam.* **38**, 475-
- 318 493 (2012).
- 319 21. Brönnimann, S. *et al.* A global historical ozone data set and prominent features of stratospheric variability prior to 1979.
- 320 *Atmos. Chem. Phys.* **13**, 9623-9639 (2013).
- 321 22. Schneider, T., Bischoff, T., & Haug, G. H. Migrations and dynamics of the Intertropical Convergence Zone. *Nature* **513**, 45-
- 322 53 (2014).
- 323 23. Bretherton, C. S., Widmann, M., Dymnikov, V. P., Wallace, J. M. & Bladé, I. The Effective Number of Spatial Degrees of
- 324 Freedom of a Time-Varying Field. *J. Clim.* **12**, 1990-2009 (1999).
- 325 24. Schraner, M. *et al.* Technical Note: Chemistry-climate model SOCOL: version 2.0 with improved transport and
- 326 chemistry/microphysics schemes. *Atmos. Chem. Phys.* **8**, 5957-5974 (2008).
- 327 25. Rayner, N. A. *et al.* Global analyses of SST, sea ice and night marine air temperature since the late nineteenth century. *J.*
- 328 *Geophys. Res.* **108**, 4407 (2003).
- 329 26. Fischer, A. M. *et al.* Interannual-to-Decadal Variability of the Stratosphere during the 20th Century: Ensemble Simulations
- 330 with a Chemistry-Climate Model. *Atmos. Chem. Phys.* **8**, 7755-7777 (2008).
- 331 27. Biasutti, M., Held, I. M., Sobel, A. H., & Giannini, A. SST forcings and Sahel rainfall variability in simulations of the 20th
- 332 and 21st centuries. *J. Clim.* **21**, 3471-3486 (2008).
- 333 28. Martin, E. R., Thorncroft, C. & Booth, B. B. B. The Multidecadal Atlantic SST—Sahel Rainfall Teleconnection in CMIP5
- 334 Simulations. *J. Clim.* **27**, 784–806 (2014).
- 335 29. Sutton, R. T. & Dong, B. Atlantic Ocean influence on a shift in European climate in the 1990s. *Nature Geosci.* **5**, 88–792
- 336 (2012).
- 337 30. Nigam, S., Guan, B. & Ruiz-Barradas, A. Key role of the Atlantic Multidecadal Oscillation in 20th century drought and wet
- 338 periods over the Great Plains. *Geophys. Res. Lett.* **38**, L16713 (2011).
- 339 31. Mohino, E., Janicot, S., Bader, J. Sahel rainfall and decadal to multi-decadal sea surface temperature variability. *Clim. Dyn.*
- 340 **37**, 419–440 (2011).

- 341 32. Knight, J. R., Folland, C. K. & Scaife, A. A. Climate impacts of the Atlantic Multidecadal Oscillation. *Geophys. Res. Lett.* **33**,  
342 L17706 (2006).
- 343 33. Booth, B. B. B., Dunstone, N. J., Halloran, P. R., Andrews, T. & Bellouin, N. Aerosols implicated as a prime driver of  
344 twentieth-century North Atlantic climate variability. *Nature* **484**, 228-232 (2012).
- 345 34. Zhang, R. *et al.* Have Aerosols Caused the Observed Atlantic Multidecadal Variability? *J. Atmos. Sci.* **70**, 1135–1144 (2013).
- 346 35. Kawase, H. *et al.* Physical mechanism of long-term drying trend over tropical North Africa. *Geophys. Res. Lett.* **37**, L09706  
347 (2010).
- 348 36. Ackerley, D. *et al.* Sensitivity of Twentieth-Century Sahel Rainfall to Sulfate Aerosol and CO<sub>2</sub> Forcing. *J. Clim.* **24**, 4999–  
349 5014 (2011).
- 350 37. Ridley, H. E. *et al.* Aerosol forcing of the position of the intertropical convergence zone since ad 1550. *Nature Geosci* **8**,  
351 195–200 (2015).
- 352 38. Compo, G. P. & Sardeshmukh, P. D. Removing ENSO-related variations from the climate record. *J. Clim.* **8**, 1957-1978  
353 (2010).
- 354 39. Allan, R. *et al.* The international atmospheric circulation reconstructions over the Earth (ACRE) initiative. *B. Amer. Meteorol.*  
355 *Soc.* **92**, 1421-1425 (2011).
- 356 40. Uppala, S. M. *et al.* The ERA-40 reanalysis. *Q. J. R. Meteorol. Soc.* **131**, 2961–3012 (2005).
- 357 41. Bodeker, G. E., Hassler, B., Young, P. J. & Portmann, R. W. A vertically resolved, global, gap-free ozone database for  
358 assessing or constraining global climate model simulations. *Earth Syst. Sci. Data* **5**, 31–43 (2013).
- 359 42. Schneider, U., *et al.* GPCP's new land surface precipitation climatology based on quality-controlled in situ data and its role in  
360 quantifying the global water cycle. *Theor. Appl. Climatol.* **115**, 15–40 (2014)
- 361 43. Brönnimann, S., Xoplaki, E., Casty, C. Pauling, A. & Luterbacher, J. ENSO influence on Europe during the last centuries.  
362 *Clim. Dynam.* **28**, 181-197 (2007).

363

## 364 **Acknowledgements**

365 The authors wish to acknowledge support by the Swiss National Science Foundation (projects EVALUATE, FUPSOL2), EU FP7  
366 project ERACLIM-2, and ERC Grant TITAN. Support for the Twentieth Century Reanalysis Project dataset is provided by the  
367 U.S. Department of Energy, Office of Science Innovative and Novel Computational Impact on Theory and Experiment (DOE  
368 INCITE) program, and Office of Biological and Environmental Research (BER), and by the National Oceanic and Atmospheric  
369 Administration Climate Program Office. We wish to thank all data providers and two anonymous reviewers for helpful  
370 comments.

371

## 372 **Corresponding author**

373 Please address correspondence to Stefan Brönnimann ([stefan.broennimann@giub.unibe.ch](mailto:stefan.broennimann@giub.unibe.ch))

374

## 375 **Author contributions**

376 SB designed the study, conducted most analyses and prepared the manuscript. AMF and ER performed the model simulations. PP  
377 provided data sets and conducted wind analyses. GPC and PDS provided data sets and suggested some of the analyses. All  
378 authors assisted in the interpretation of the data, discussed results and commented on the manuscript.

379

## 380 **Data sources**

381 20CR and 20CR v2c can be downloaded from [http://www.esrl.noaa.gov/psd/data/20thC\\_Rean/](http://www.esrl.noaa.gov/psd/data/20thC_Rean/)

382 ERA-20C can be downloaded from <http://apps.ecmwf.int/datasets/data/era20c-daily/>

383 REC1 and REC2 are available from the Bern Open Repository (BORIS) at <http://boris.unibe.ch/id/eprint/71204> with further  
384 information and details from <http://www.oeschger.unibe.ch/research/databases/CHUAN/>

385 HISTOZ is available from the Bern Open Repository (BORIS) at <http://boris.unibe.ch/id/eprint/39429>

386 ICOADS can be downloaded from <http://rda.ucar.edu/datasets/ds540.0/>

387 HadISST1.1 can be downloaded from <http://www.metoffice.gov.uk/hadobs/hadisst/>

388 GPCC can be downloaded from <http://www.esrl.noaa.gov/psd/data/gridded/data.gpcc.html>

389 SOCOL simulations are available from the Bern Open Repository (BORIS) at <http://boris.unibe.ch/id/eprint/71204>

390

## 391 **Code availability**

392 The R code used to calculate the indices are available from the Bern Open Repository (BORIS) at

393 <http://boris.unibe.ch/id/eprint/71204>

394 For simple operations such as interpolation, masking, extraction, averaging, and standard statistics (linear least-squares  
395 regression, correlation, calculation of degrees of freedom) standard packages of R were used.

396

## 397 **Additional Information**

398 Supplementary information is available in the online version of the paper.

399

## 400 **Competing financial interests**

401 The authors declare no competing financial interests.

402 **Figure captions**

403

**ITCZ**

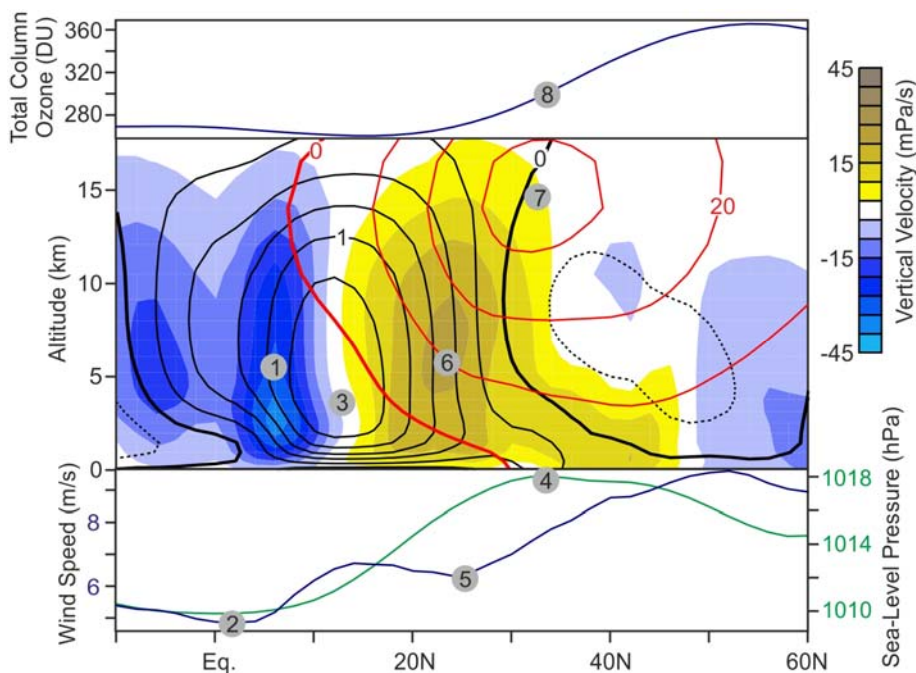
- ① Strongest Ascent  
(Max. 500 hPa Upward Velocity)
- ② Equatorial Calms  
(Min. Marine Wind Speed)

**Hadley Cell Centre**

- ③ Centre of Overturning Circulation  
(Max. Stream Function)

**Northern Tropical Edge**

- ④ Subtropical Highs  
(Max. Sea-Level Pressure)
- ⑤ Subtropical Calms  
(Min. Marine Wind Speed)
- ⑥ Strongest Descent  
(Max. 500 hPa Downward Velocity)
- ⑦ Subtropical Jet  
(Max. 200 hPa Zonal Wind)
- ⑧ Subtropical Ozone Front  
(Max. Poleward Total Column Ozone Increase)



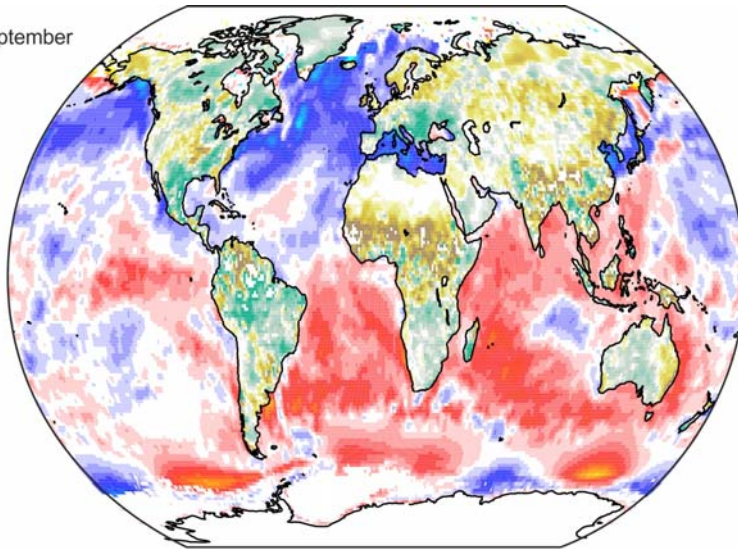
404

405

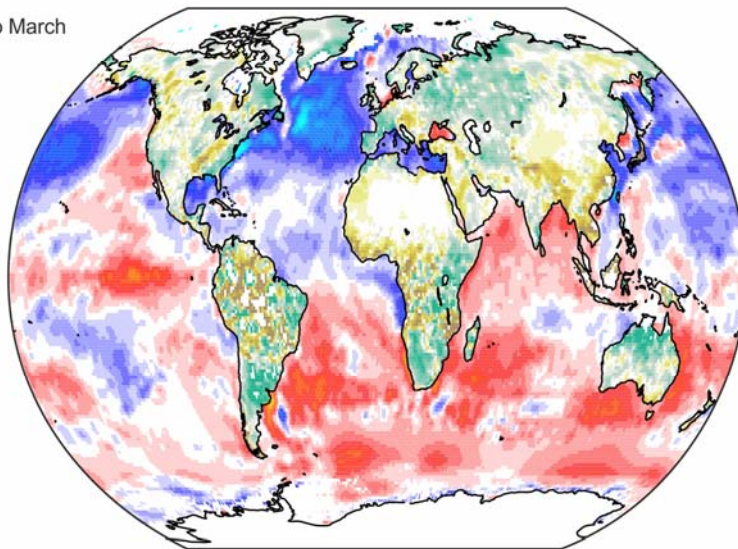
406 **Figure 1: Schematic diagram of the tropical edge and measures of its position.** Contours show the  
 407 1945-1980 climatology of the zonal mean zonal wind (red, m/s) and the zonal mean meridional stream  
 408 function (black,  $10^9$  kg/s) in boreal winter from the 20CR reanalysis v2c. The shading represents the  
 409 climatological vertical velocity (mPa/s). The top and bottom panels show zonal mean total column ozone,  
 410 sea-level pressure (both from 20CR v2c) and marine 10 m wind speed (ERA20C).



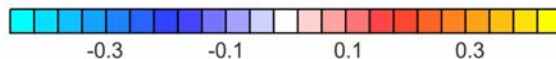
April to September



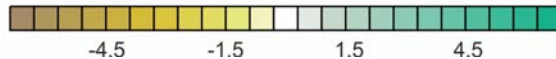
October to March



Temperature Trend  
(°C per decade)



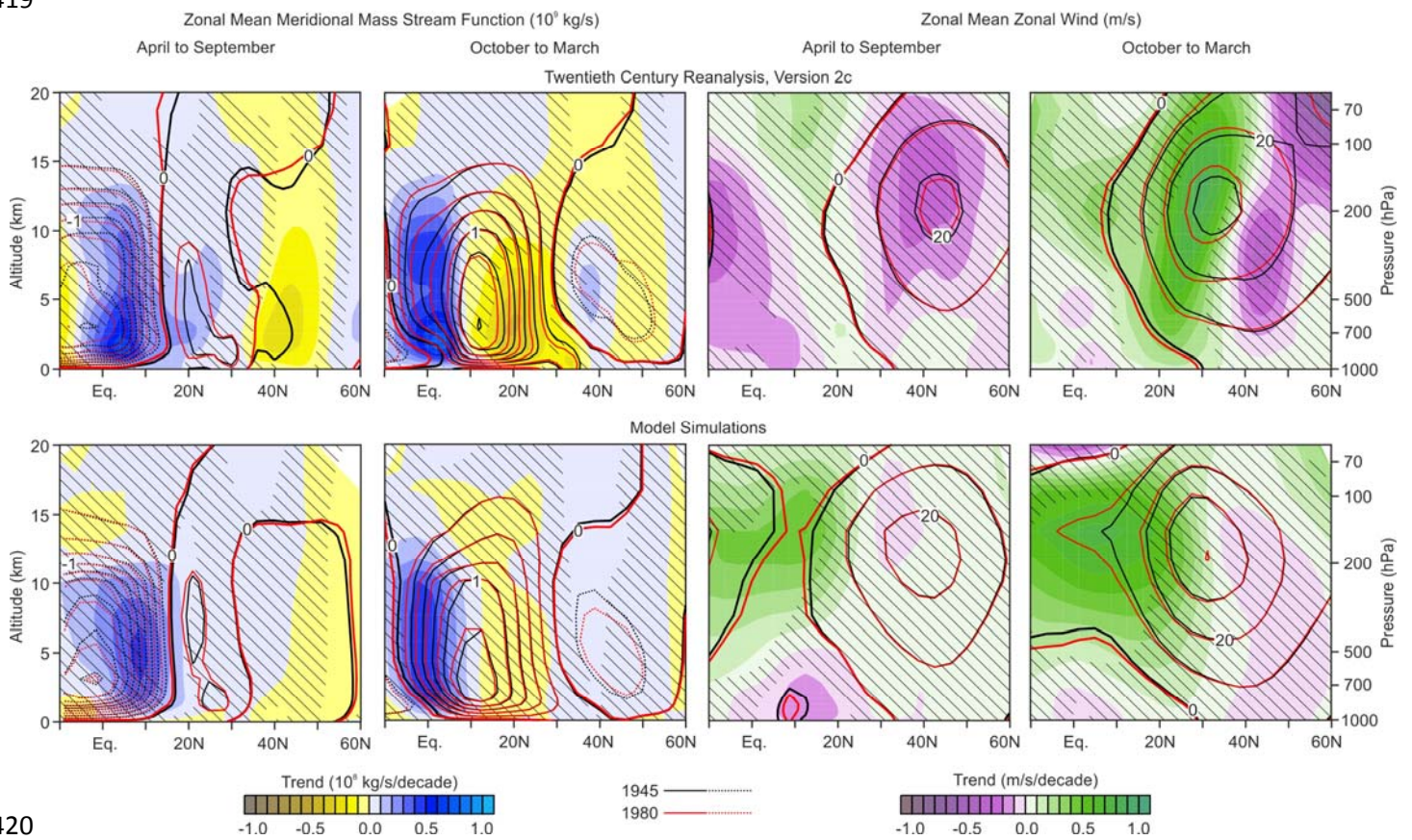
Precipitation Trend  
(mm/mon per decade)



411  
412

413 **Figure 2: Trends in sea-surface temperature and land precipitation from observations, 1945-1980.**

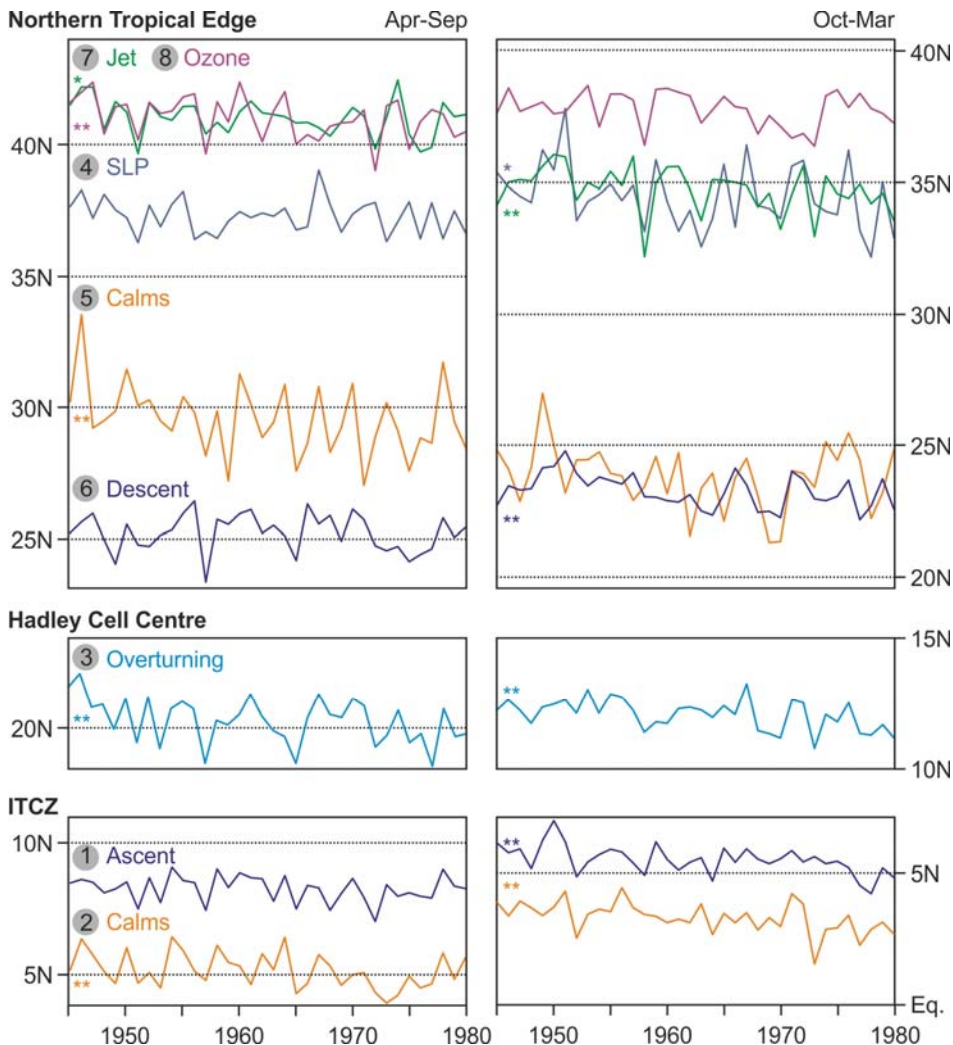
414 Trends were calculated with least squares regression from seasonal averages of sea-surface  
415 temperature<sup>25</sup> (HadISST1.1) and precipitation (GPCC reanalysis Version 6)<sup>42</sup>. Boreal summer  
416 precipitation trends are significant over the Sahel region and southeastern Europe, sea-surface  
417 temperature trends are significant over most of the Atlantic, Indian and Southern Oceans (see Fig. S1 for  
418 trend significance).



420

421 **Figure 3: Latitude-height cross section of trends in the zonal and meridional circulation, 1945-**  
 422 **1980.** Contours show the trend fit of the zonal mean meridional mass stream function (left) and the zonal  
 423 mean zonal wind (right) in boreal summer and winter for the years 1945 (black) and 1980 (red). Shading  
 424 shows trends over the 1945 to 1980 period (hatching means not significant at  $p < 0.05$ ). The top row is  
 425 based on 20CR v2c, the bottom row on the ensemble mean of the SOCOL “all forcings” simulations.

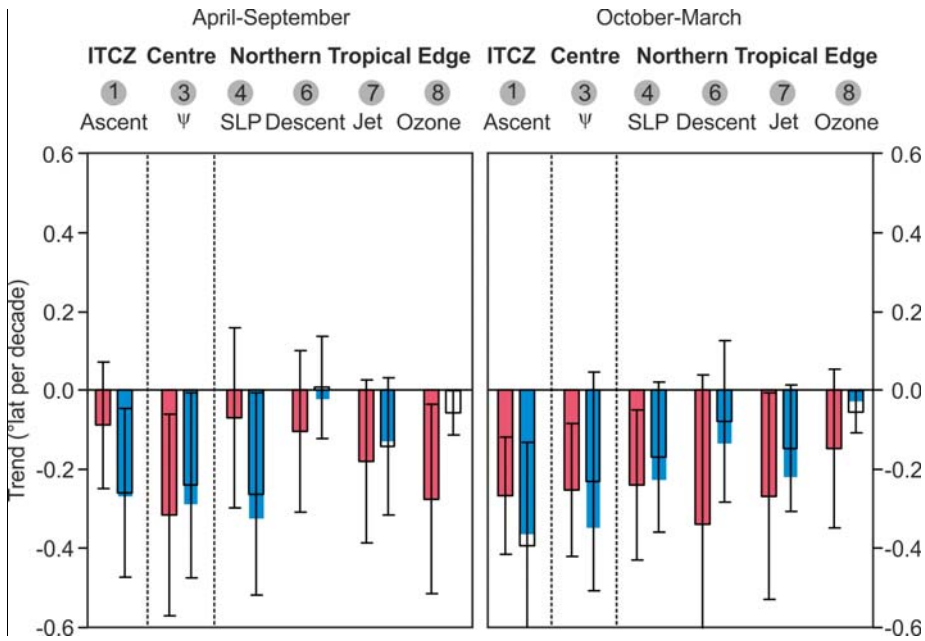
426



427  
428

429 **Figure 4: Changes in the northern tropical belt.** Time series of the latitude of the northern tropical edge  
 430 (defined by the subtropical jet, the largest total column ozone meridional gradient, the maximum sea-level  
 431 pressure, maximum descent and subtropical calms), the Hadley Cell centre (max. meridional stream  
 432 function) and the Intertropical Convergence Zone (ITCZ, max. 500 hPa upward velocity) in (left) April to  
 433 September and (right) October to March. See Fig. 1 for an explanation of the indices. Trends in these  
 434 series that are significant at the 90% and 95% confidence limits, are marked with \* and \*\*, respectively.

435  
436



437  
438

439 **Figure 5: Trends in the latitudinal position of the northern tropical belt in observation-based data**  
 440 **and model simulations, 1945-1980.** Trends are for the position of the ITCZ (maximum ascent), the  
 441 Hadley cell centre and four indices for the northern tropical edge (see Fig. 1 for an explanation of the  
 442 indices). The observation-based trends are shown as filled red bars, those of the “all forcings” simulations  
 443 as empty bars. Whiskers indicate 95% confidence intervals of the trend. The contribution of sea-surface  
 444 temperature (blue boxes) indicates the difference in the trends between the “all forcings” simulations and  
 445 an ensemble of 3 simulations with sea-surface temperature held constant.